ACS APPLIED MATERIALS & INTERFACES

Research Article

www.acsami.org

Preparation of Flexible Organic Solar Cells with Highly Conductive and Transparent Metal-Oxide Multilayer Electrodes Based on Silver Oxide

Jungheum Yun,*[,†] Wei Wang,[†,‡] Tae Sung Bae,[§] Yeon Hyun Park,[†] Yong-Cheol Kang,[∥] Dong-Ho Kim,[†] Sunghun Lee,[†] Gun-Hwan Lee,[†] Myungkwan Song,*[,†] and Jae-Wook Kang*[,⊥]

[†]Surface Technology Division, Korea Institute of Materials Science, Changwon, Gyeongnam 641-831, Republic of Korea

[‡]Key Laboratory for Liquid−Solid Structural Evolution and Processing of Materials, Shandong University, Jinan 250061, China

[§]Jeonju Center, Korea Basic Science Institute, Jeonju, Jeonbuk 561-180, Republic of Korea

[∥]Department of Chemistry, Pukyong National University, Busan 608-737, Republic of Korea

[⊥]Professional Graduate School of Flexible and Printable Electronics, Department of Flexible and Printable Electronics, Chonbuk National University, Jeonju, Jeonbuk 561-756, Republic of Korea

Supporting Information

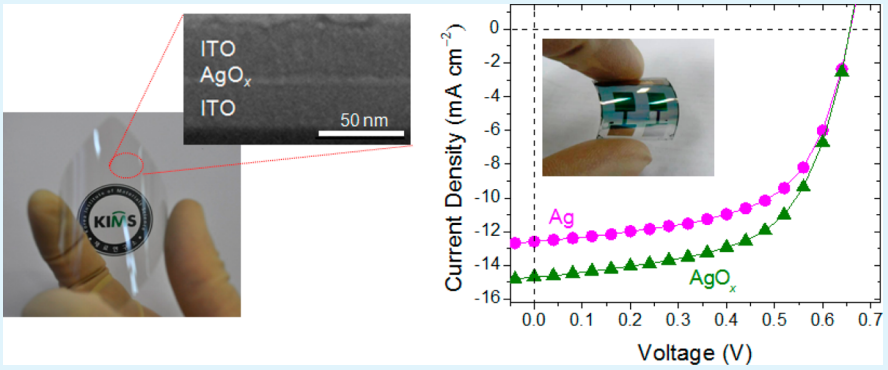

ABSTRACT: We report that significantly more transparent yet comparably conductive AgO_x films, when compared to Ag films, are synthesized by the inclusion of a remarkably small amount of oxygen (i.e., 2 or 3 atom %) in thin Ag films. An 8 nm thick AgO_x (O/Ag = 2.4 atom %) film embedded between 30 nm thick ITO films (ITO/AgO_x/ITO) achieves a transmittance improvement of 30% when compared to a conventional ITO/Ag/ITO electrode with the same configuration by retaining the sheet resistance in the range of 10−20 Ω sq^{-1}. The high transmittance provides an excellent opportunity to improve the power-conversion efficiency of organic solar cells (OSCs) by successfully matching the transmittance spectral range of the electrode to the optimal absorption region of low band gap photoactive polymers, which is highly limited in OSCs utilizing conventional ITO/Ag/ITO electrodes. An improvement of the power-conversion efficiency from 4.72 to 5.88% is achieved from highly flexible organic solar cells (OSCs) fabricated on poly(ethylene terephthalate) polymer substrates by replacing the conventional ITO/Ag/ITO electrode with the ITO/AgO_x/ITO electrode. This novel transparent electrode can facilitate a cost-effective, high-throughput, room-temperature fabrication solution for producing large-area flexible OSCs on heat-sensitive polymer substrates with excellent power-conversion efficiencies.

KEYWORDS: *flexible electrode, organic solar cell, silver oxide, transparent conducting electrode, polymer substrate*

1. INTRODUCTION

It is desirable to fabricate highly flexible electrodes with high electrical conductivities and optical transparencies on polymer substrates for use in flexible optoelectronic and photonic devices. However, this goal is unrealizable using the most commonly employed transparent conductive oxide (TCO) material at present, namely, indium tin oxide (ITO), owing to its mechanical brittleness and poor electrical conductivity. Oxide−metal−oxide (OMO) hybrid electrodes have received attention as potential alternatives[1−7] along with metal nanopatterns[8] and nanowires,[9−11] carbon nanotubes,[12−14] graphenes,[15−17] and metal-oxide-based nanowires.[18−20] OMO electrodes have relative advantages over the other alternatives in terms of the fabrication methodology because the electrodes can be fabricated via relatively mature and scalable technologies such as vacuum sputtering at room temperature, allowing for a high-

Received: May 16, 2013
Accepted: September 23, 2013
Published: September 23, 2013

throughput roll-to-roll production of such electrodes on large-area polymer substrates. In OMO electrodes, a highly conductive metal layer with a thickness of about 10 nm, which is close to the threshold thickness for achieving a continuous layer, is embedded between layers of oxides that are either conductive or dielectric in nature and a few tens of nanometers in thickness. A sheet resistance of approximately 10−20 Ω sq^{-1} is readily attainable with an overall layer thickness of less than 100 nm. The relatively thin top and bottom oxide films and the ductility of the sandwiched metal layer result in a higher structural durability of the electrodes than that observed for conventional single-film-type TCO electrodes.[1] However, OMO electrodes have not found wide application in flexible optoelectronic and photonic devices because the sandwiched metal layer tends to strongly reflect incident light in the visible and near-infrared regions. The high degree of reflection exhibited by the metal layer, which leads to a significant reduction in the transmittance of OMO electrodes, is an inherent optical property of metals and may not be suppressed sufficiently by merely ensuring optical matching between the metal and the oxide layers. Varying the optical characteristics of the metal itself is seen as the only way of reducing the degree of reflection, although no credible solution incorporating this technique has yet been proposed.

In this study, we report that the transmittance of a thin Ag film embedded in an OMO electrode can be improved significantly via the oxidation of the Ag film to a minimal degree, without any noticeable degradation in the electrical conductivity of the OMO electrode. It is generally agreed that the oxidation of Ag films, which leads to a noticeable improvement in their optical transmittance, unavoidably results in a severe degradation of their electrical conductivity.[21−23] The transition of Ag to its highly oxidized, dielectric phases, which predominantly comprise Ag_2O and AgO, has been routinely exploited for improving the optical transmittance characteristics of Ag films.[23−26] However, there have been no previous studies on the synthesis of AgO_x thin films via the minimal oxidation of Ag films. Hence, the fact that the AgO_x thin films formed are less refractive than, but as conductive as, the Ag films is little understood. In this study, it was possible to achieve such an improvement in optical transmittance using ITO/AgO_x/ITO electrodes, which also exhibited other desirable physical characteristics, such as a low electrical conductivity of about 10 Ω sq^{-1} and an excellent structural flexibility. These properties of ITO/AgO_x/ITO electrodes were verified by using the electrodes to fabricate highly efficient and flexible organic solar cells (OSCs) on poly(ethylene terephthalate) (PET) substrates. Significant improvements in the power-conversion efficiency (PCE) of the OSCs could be achieved by successfully matching the transmission spectral range of the electrodes with the optimal absorption region of low band gap photoactive polymers within the OSCs. The power-conversion efficiency of the OSCs fabricated using the OMO electrodes increased from 4.72 to 5.88% when the 8 nm thick Ag film in the OMO electrode was replaced with an AgO_x (O/Ag = 2.4 atom %) film of the same thickness.

2. EXPERIMENTAL METHODS

2.1. Electrode Fabrication. The ITO/Ag/ITO and ITO/AgO_x/ITO electrodes were deposited on 75 μm thick PET polymer substrates (Panac Co. Ltd.) by sputtering processes. The bottom and top 30 nm thick ITO films were deposited via a home-built radio frequency (RF) (13.56 MHz) magnetron sputtering system using an ITO target (Advanced Nano Products Co. Ltd.) composed of In_2O_3 with 3 wt % Sn. The chamber was initially evacuated to 6.7×10^{-4} Pa prior to the sputtering, and the chamber pressure was then increased to 0.31 Pa by introducing Ar gas (99.9999%) at a flow rate of 22 sccm. The sputtering process was carried out at an RF power of 0.53 W cm^{-2} and room temperature. The Ag and AgO_x films of different thicknesses were deposited using a separate direct current (dc) reactive magnetron sputtering system (Flexlab System 100, A-Tech System Co.) with a 10.2 cm Ag target (Williams Advanced Material Inc.) at a dc power of 0.1 W cm^{-2}. The chamber pressure was kept at 0.4 Pa by introducing pure Ar gas at a flow rate of 45 sccm for the Ag sputtering processes and a mixture of Ar and O_2 gases, with the O_2 gas being added at a flow rate between 4 and 12 sccm, for the AgO_x sputtering processes. The Ag and AgO_x films were exposed to the ambient atmosphere for at least tens of minutes before top ITO deposition.

2.2. OSC Fabrication. The electrodes were used as the anode in the OSCs with the following configuration: PET/anode/PEDOT-PSS/PTB7-F20:PC_{71}BM/Al-cathode. A 45 nm thick layer of PEDOT-PSS (Clevious P) was coated on the electrodes by spin coating (5000 rpm for 40 s) a solution of PEDOT-PSS diluted with isopropyl alcohol (IPA), with the dilution ratio being 1:2. The coated buffer layer was cured at a temperature of 100 °C for 5 min. A 100 nm thick active layer of PTB7-F-20:PC_{71}BM was spin coated (1000 rpm for 40 s) using a mixture of PTB7-F20:PC71BM (8:12 mg) that was dissolved in 1 mL of chlorobenzene and further mixed with 1,8-diiodooctane (3%, v/v) (Sigma-Aldrich). The compounds PTB7-F20 and PC71BM were purchased from 1-Material and Solemme BV, respectively. A 100 nm thick Al cathode with a defined area of 0.36 cm^2 was deposited via evaporation on the active layer.

2.3. Characterization. The oxygen concentrations of the Ag and AgO_x films were determined using XPS (VG Scientific, Escalab 200R) using an Al Kα (1486.6 eV) X-ray source at 250 W (12.5 kV and 20 mA) and a concentric hemispherical analyzer with a scan pass energy of a 100 eV. The refractive indices of the Ag and AgO_x films with a thickness of 20 nm were determined using spectroscopic ellipsometry (Ellipso Technology, Elli-SEU-am12) measurements performed using the Lorentz oscillator dispersion model. The measurements were made at an angle of incidence of 70° over the energy range 1.2−5.2 eV. The crystallographic data of the Ag and AgO_x films were determined using XRD (PANalytic, X'pert MPD) by using the Cu Kα line for the X-ray source. The sheet resistances of the Ag and AgO_x films deposited on glass substrates as well as those of the ITO/Ag/ITO and ITO/AgO_x/ITO electrodes deposited on PET substrates were measured using a four-point probe system (Mitsubishi Chemical Co., MCP-T600). The average values of the sheet resistance were calculated using the values of at least three different 3×3 cm^2 samples of each electrode type. The carrier concentrations and hole mobilities of the ITO/Ag/ITO and ITO/AgO_x (O/Ag = 2.4 atom %)/ITO electrodes were determined from 1×1 cm^2 samples of the electrodes using a Hall effect measurement system (HMS-3000, Ecopia) and the van der Pauw method. The cross-sectional and surface morphologies of these electrodes were determined using UHR FE-SEM (S-5500, Hitachi Co.), whereas the surface morphologies were also determined for 8 nm thick Ag and AgO_x (O/Ag = 2.4%) films deposited on 30 nm thick ITO films. The film thicknesses of the Ag, AgO_x, ITO layers were measured using either spectroscopic ellipsometry or a surface profiler (KLA-Tencor, P-11). The total and specular spectra of the electrodes were determined using an ultraviolet−visible (UV−vis) spectrophotometer (Cary 5000, Varian) with normally incident radiation at wavelengths between 320 and 800 nm. The characteristics of the OSCs were determined from their $J-V$ curves, which were determined using a Keithley 2400 SourceMeter source measurement unit, and their IPCE spectra, which were determined using a quantum efficiency measurement system (Oriel IQE-200) with a 250 W quartz tungsten halogen (QTH) lamp as its light source, were determined under simulated AM 1.5G illumination with an irradiance of 100 mW cm^{-2}. These values were averaged over five different OSC samples. The UV photoelectron emission was measured by UPS using a gas-discharge UV source housed at ESCALAB MKII, He I radiation ($h\nu$ = 21.2 eV) with a pass-energy of 50 eV. The low-energy secondary electron cutoff

was observed by applying a takeoff angle of 45° relative to the sample surface. The flexibilities of both the electrodes and the OSCs were measured as a function of the bending radius, which was approximately half of the distance between the two plates of a custom-made irreversible bending system. The bending strain (ε) was approximated by the relation $\varepsilon = H/(2R)$, where H is the substrate thickness and R is the bending radius.[27]

3. RESULTS AND DISCUSSION

Large variations in the optical properties of the Ag film were noticed for low levels of Ag oxidation. The introduction of oxygen in extremely small concentrations (2.4 atom % in this case) caused significant improvements in the transmittance of thin single-AgO_x films compared to those of single-Ag films that were deposited on PET substrates (Figure 1a). The increase in

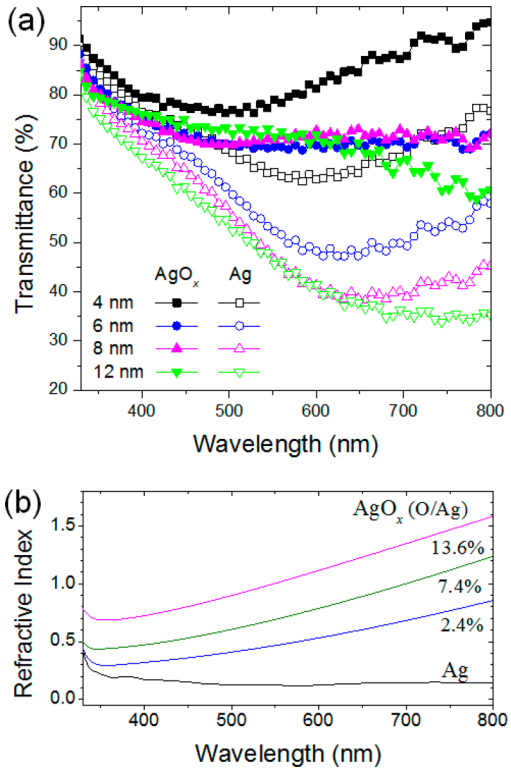

Figure 1. (a) Differences in the optical transmittance of single-Ag films and single-AgO_x (O/Ag = 2.4 atom %) films with different film thicknesses deposited on PET substrates, which were precoated with 20 nm thick Al_2O_3 films to promote the adhesion of the Ag and AgO_x films with the inert surface of the polymer substrates. (b) Effects of the variations in the O/Ag atomic ratios of AgO_x films on their refractive indices.

the oxygen concentration of the AgO_x films led to a significant increase in their refractive index values, which were evaluated via spectroscopic ellipsometry measurements performed in the visible-wavelength range (Figure 1b). A truly interesting point to note here is that the inclusion of even small amounts of oxygen in the AgO_x films led to a significant increase in their refractive index values, much higher than those of Ag films. The change in the refractive index of the AgO_x films could be readily attributed to the inclusion of highly transparent oxidized phases in the Ag domain. The difference in the refractive index values of the Ag and AgO_x (O/Ag = 2.4 atom %) films was even greater for longer wavelengths. Given that the refractive index of the surface of PET films for a wavelength of 550 nm is about 1.77, the replacement of Ag with AgO_x (O/Ag = 2.4 atom %) led to a decrease in the degree of light reflection by the AgO_x films owing to the diminution of a radical change in the refractive index with respect to the path of light propagation through the electrode. Although the refractive index value of the AgO_x films could be increased further with an increase in the oxygen concentration to values much greater than 2.4 atom %, these higher oxygen concentrations might not be suitable because they resulted in degradation, to some degree, in the conductivity of the AgO_x films (Figure 2a). This degradation in the electrical conductivity of the AgO_x films with increasing the oxygen concentration could be readily explained by significant degradations in the crystallographic phases of the metallic Ag film, which were observed by X-ray diffraction (XRD) measurements (Figure 2b). The peak of irregular amorphous oxide phases intensified as the oxygen concentration increased during the sputtering process. When the oxygen concentrations of the AgO_x films were determined using X-ray photoelectron spectroscopy (XPS), the atomic ratio O/Ag of the bulk of the AgO_x films increased almost linearly with an increase in the flow of O_2 gas during the sputtering process (Figure 2c).

A comparison of the total and specular transmittance of the single-Ag and AgO_x films confirmed that a detectable but not significant difference between the total and specular transmittance was observed for the Ag and AgO_x (O/Ag = 2.4%) films, indicating that the scattering of incident light in the films was not significant (see Figure S1 in the Supporting Information). The difference in the transmittance increased for larger O/Ag ratios of AgO_x films, although the difference did not exceed 5%. However, there was a much larger (and significant) difference between the total and specular reflections of the Ag and AgO_x films when compared with the difference between the total and specular transmittance. The 10 nm thick Ag film exhibited a total reflection that was 10% greater than its specular reflection; this was the result of an increase in light scattering owing to a rough and granular surface morphology of the thin Ag film. Interestingly, the difference was reduced by the increase in the O/Ag ratio of the AgO_x films of the same thickness. Furthermore, the larger scattering in the reflection of light than that in the transmittance can be readily explained by the term dipole radiation. It is not unreasonable to suppose that the light scattering by Ag or AgO_x thin films with granular morphologies is a dipole radiation. When a dipole is placed on a substrate that has a larger refractive index than the medium covering the dipole, the radiation by the dipole is mainly into the substrate.[28] In this study, the substrate and the covering medium were PET and air, respectively. Therefore, the scattering in the reflection by the Ag and AgO_x films through the PET substrate was stronger than that in the transmittance.

A comparison of the morphological characteristics of the ITO/Ag/ITO and ITO/AgO_x (O/Ag = 2.4%)/ITO electrodes, performed using the results of ultra-high-resolution (UHR) field-emission scanning electron microscopy (FE-SEM), disclosed that the insertion of a AgO_x film between the 30 nm thick ITO films led to a significant improvement in the morphology of the top ITO film subsequently deposited on the AgO_x film (Figure 3). Although the Ag and AgO_x films both covered the bottom ITO films incompletely at a film thickness of 8 nm, a mitigation of 3D and granular morphology was observed in the top ITO film deposited on the AgO_x films (Figure 3e–h). The highly granular morphology was confirmed to cause a significant number of nanoscaled pinholes and grain boundaries between the ITO granules deposited on the Ag

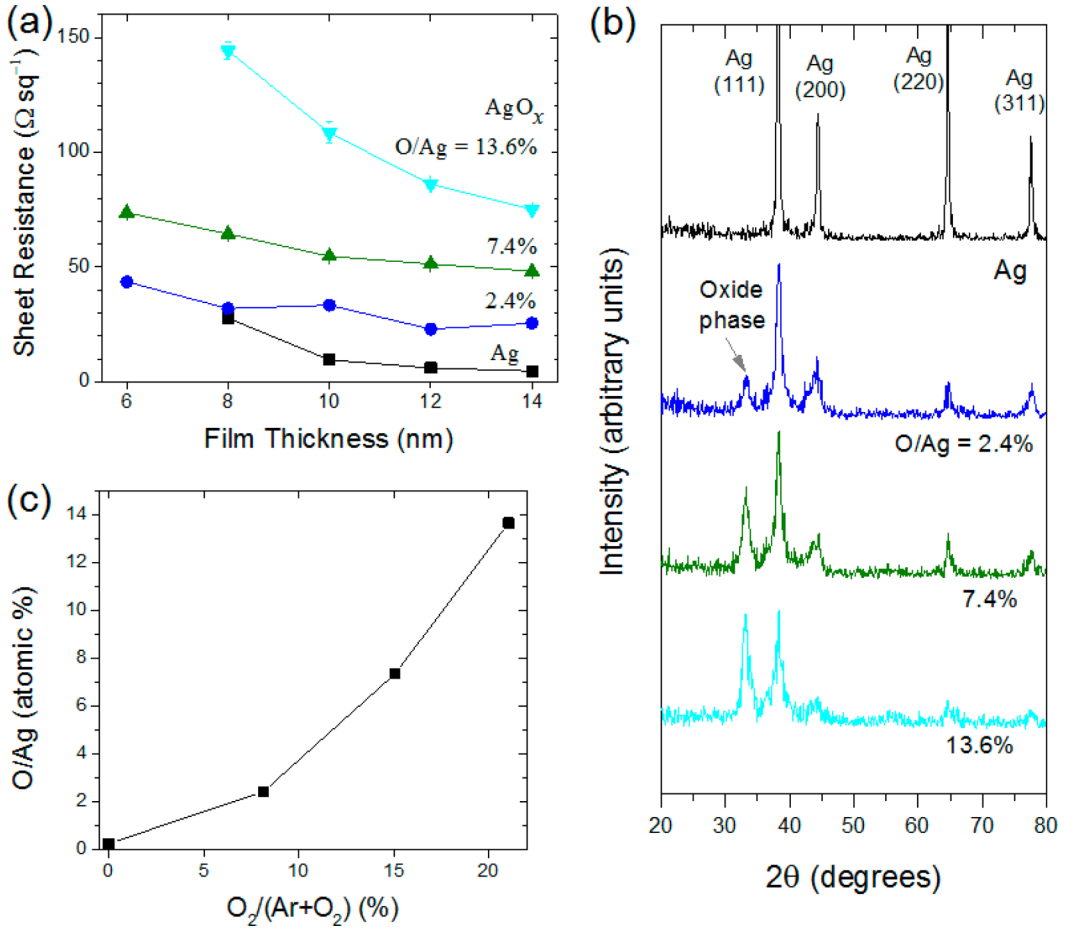

Figure 2. Dependence of (a) the sheet resistances and (b) XRD patterns of Ag and AgO_x films on their O/Ag atomic ratios. (c) Dependence of the O/Ag atomic ratios of AgO_x films on the flow of O_2 gas during the sputtering process at room temperature. The concentrations of O and Ag were determined from the O 1s and Ag 3d XPS spectra, respectively.

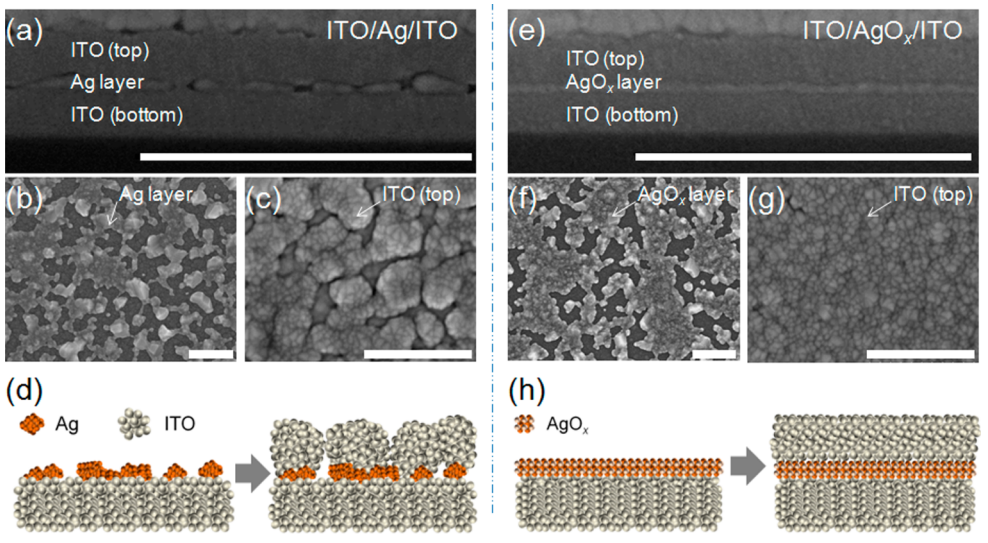

Figure 3. Differences in the morphologies of the (a–d) ITO/Ag/ITO and (e–h) ITO/AgO_x/ITO electrodes. Top-view FE-SEM images showing (b) Ag and (f) AgO_x (O/Ag = 2.4 atom %) films with a thickness of 8 nm deposited on 30 nm thick ITO films. Cross-sectional and top-view images showing 30 nm thick ITO films deposited on Ag and AgO_x films to form the (a, c) ITO/Ag/ITO and (e, g) ITO/AgO_x/ITO electrodes. Schematic diagrams illustrating the difference in the morphological evolution between the (d) ITO/Ag/ITO and (h) ITO/AgO_x/ITO electrodes. Scale bars correspond to 200 nm.

films (Figure 3a–d). This undesirable morphology seems to be an inherent property of ITO films deposited on thin Ag films because a similar morphology was observed even after the thickness of the Ag film was increased to 12 nm (see Figure S2

dx.doi.org/10.1021/am401845n | ACS Appl. Mater. Interfaces 2013, 5, 9933–9941

in the Supporting Information). The morphological differences between the ITO films deposited on Ag and AgO_x films could be primarily explained by strong influences of the discontinuity and granularity states of the Ag and AgO_x films on the ITO morphologies. The lateral expansion of ITO granules along the top surface of the Ag films was restricted because of the large numbers of grain boundaries and voids in the Ag films. As a result, there was a serious delay in the coalescences of neighboring ITO granules, leading to continuous layer formation. However, the inferior morphology of the top ITO films because of the delay in continuous layer formation was largely reduced by forming less granular and more continuous AgO_x films at the same thickness.

The superior morphology of the ITO/AgO_x (O/Ag = 2.4 atom %)/ITO electrode fully compensated for the fact that the conductivity of AgO_x is lower than that of Ag (Figure 4). The

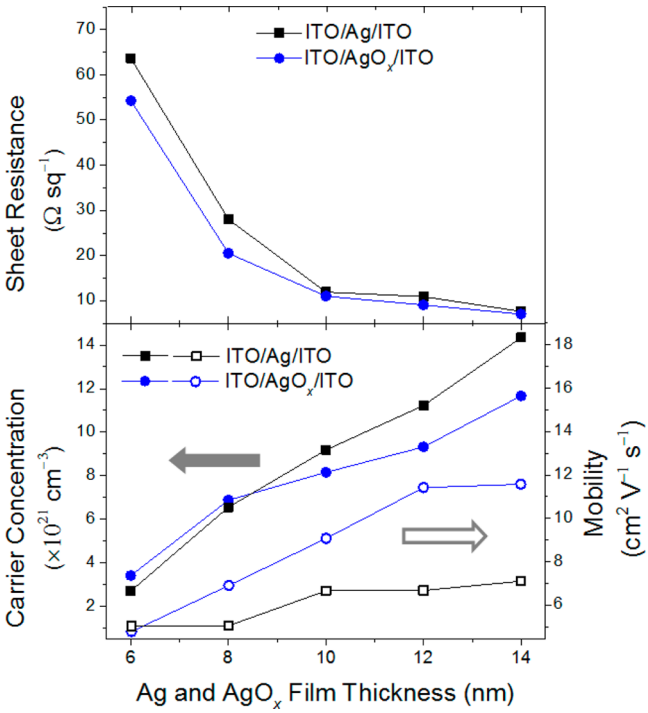

Figure 4. Differences in the sheet resistance (upper figure, full symbols), carrier concentration (lower figure, full symbols), and mobility (lower figure, open symbols) values of ITO (30 nm)/Ag/ITO (30 nm) and ITO (30 nm)/AgO_x/ITO (30 nm) with different Ag and AgO_x (O/Ag = 2.4 atom %) film thicknesses between 6 and 14 nm.

conductivity of the ITO/AgO_x/ITO electrode was greater than that of the ITO/Ag/ITO electrode for AgO_x film thicknesses lower than or equal to 8 nm. However, further increases in the thickness of the AgO_x film to values greater than 8 nm attenuated the effects of the improvements in morphology. The sheet resistance of the ITO/AgO_x/ITO electrode became almost similar to that of the ITO/Ag/ITO electrode, with its value reaching 10 Ω sq^{-1} (7×10^{-5} Ω cm) for Ag and AgO_x films of about 10 nm in thickness. The decrease in the sheet resistance with the increase in the thickness of the Ag and AgO_x films was mostly caused by increases in the carrier concentration and Hall mobility. This was because the discontinuous conduction paths noticed in the thinner AgO_x and Ag films were fewer in the thicker films and were eventually eliminated when continuous films were formed. Although the carrier concentration in the case of the ITO/Ag/ITO electrode increased monotonically with the thickness of the Ag film and became larger than that of the ITO/AgO_x/ITO electrode for film thicknesses greater than 8 nm, the mobility in the case of the ITO/Ag/ITO electrode was much lower than that of the ITO/AgO_x/ITO electrode for thicknesses greater than or equal to 8 nm. The scattering of carriers at the interface between the ITO and Ag films could be the primary mechanism behind the reduction in the mobility of the thinner Ag films because these Ag films formed discontinuous islandlike structures.[2,3] Scattering might not be that significant at the interface between the ITO and AgO_x films because the contact area between the ITO and AgO_x films reduced when the AgO_x films formed much larger islands owing to the rapid coalescence of smaller islands. Furthermore, the grain-boundary scattering noticed in the top ITO films, which were deposited on top of the Ag films and were 3D and highly granular in morphology, could be another reason for the fact that the mobility of the ITO/Ag/ITO electrode continued to be less than that of the ITO/AgO_x/ITO electrode even after the thickness of the Ag and AgO_x films was increased to a value that was sufficient to ensure completely continuous films. However, the sheet resistances achievable in these electrodes were still much lower than that of a 70 nm thick Ag and AgO_x free single ITO film, which was about 70 Ω sq^{-1}. The sheet resistance of the single ITO film reached 20 Ω sq^{-1} as its thickness was increased to greater than 200 nm (see Figure S3 in the Supporting Information). Single ITO films deposited on polymer substrates at room temperature or at least near room temperature exhibit higher sheet resistance and lower transmittance when compared with single ITO films deposited on glass substrates at elevated temperatures (much higher than 100 °C). The most plausible explanation for higher sheet resistance is the inclusion of highly amorphous structures and fine grains that provide negative effects on the electrical conductivity by hindering the electron mobility in the films. These inferior film properties further result in the reduction in the transmittance by promoting the scattering of incident light. Although the conductivity and transmittance of the single ITO films could be improved by increasing the film thickness from 70 nm under the process conditions used in this study, such thick ITO films were rarely considered as flexible transparent conducting electrodes in spite of better conductivity and transmittance owing to their brittleness on PET substrates.

The tuning of the refractive index of the ITO/AgO_x/ITO electrode owing to the oxidation of Ag resulted in the electrode being highly transparent in the visible spectrum, in contrast to the ITO/Ag/ITO electrode (Figure 5). The specular transmittance of the ITO/AgO_x (O/Ag = 2.4 atom %)/ITO electrode was optimal when the AgO_x film was not completely continuous and was 8 nm in thickness (Figure 5a). The optimized ITO/AgO_x/ITO electrode exhibited the maximum specular transmittance (88%) at approximately 600 nm, whereas the ITO/Ag/ITO electrode with an 8 nm thick Ag film exhibited a significant loss in transmittance, with its specular transmittance being much lower (56%) at the same wavelength. The transmittance of the ITO/AgO_x/ITO electrode decreased gradually with an increase in the wavelength to values greater than 600 nm and yet reached a value of 75% at a wavelength of 800 nm. This high transmittance at longer wavelengths could enable the production of high levels of photocurrent at longer wavelengths. The difference in the transmittance of the ITO/AgO_x/ITO and ITO/Ag/ITO

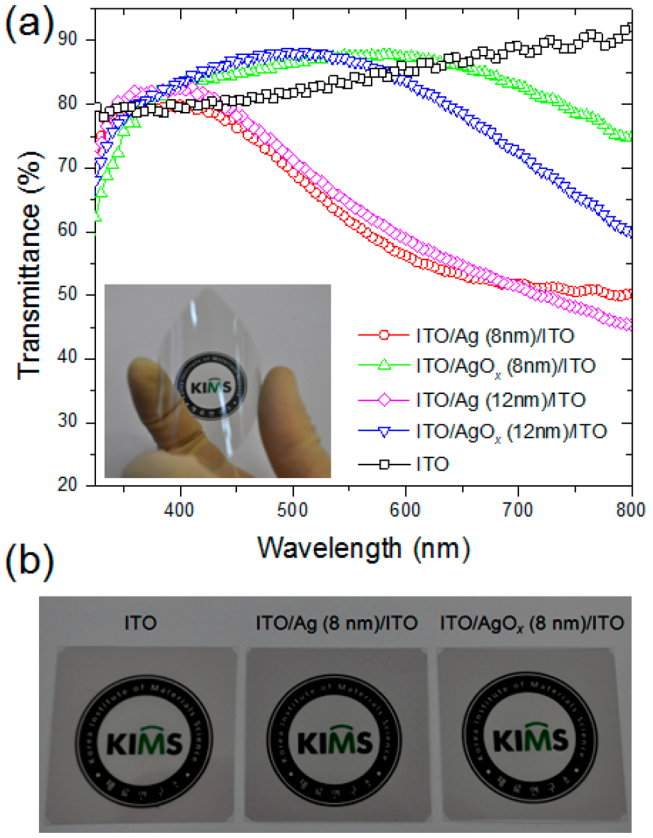

Figure 5. (a) Optical transmittance of ITO (30 nm)/Ag/ITO (30 nm), ITO (30 nm)/AgO$_x$/ITO (30 nm), and 70 nm thick single ITO film electrodes with two different Ag and AgO$_x$ (O/Ag = 2.4 atom %) thicknesses, namely, 8 and 12 nm. The transmittance values are of the electrodes alone and not of the PET substrates. A photograph of a highly flexible PET substrate coated with the optimized ITO/AgO$_x$ (8 nm)/ITO electrode is shown in the inset. (b) Photograph showing the difference in the transmittance of the ITO, ITO/Ag (8 nm)/ITO, and ITO/AgO$_x$ (8 nm)/ITO electrodes.

electrodes can be seen in the photograph shown in Figure 5b. The transmittance of the ITO/AgO$_x$/ITO electrode with an 8 nm thick AgO$_x$ film surpassed that of a single 70 nm thick ITO film for wavelengths of up to 700 nm. As the thickness of the AgO$_x$ film increased to 12 nm, the transmittance of the electrodes decreased drastically for wavelengths greater than 600 nm. However, the transmittance increased slightly for wavelengths between 400 and 500 nm.

The performance of the ITO/AgO$_x$ (O/Ag = 2.4 atom %)/ITO as a transparent conducting electrode was further evaluated by comparing a figure of merit (FoM) of the electrode with that of the ITO/Ag/ITO electrode (see Figure S4 in the Supporting Information). The FoM was relevant to the transmittance and the sheet resistance of the electrodes and was given by the following expression: FoM = T^{10}/R_s, where T is the specular transmittance and R_s is the sheet resistance of the electrodes.[29] A higher value of the FoM suggests a better performance of the transparent conducting electrode. The value of the FoM of the ITO/AgO$_x$/ITO electrode outperformed that of the ITO/Ag/ITO electrode for the entire thickness range of Ag and AgO$_x$ films examined. The values of the FoM of the ITO/AgO$_x$/ITO electrode were 8.06×10^{-3} and 2.69×10^{-2} Ω^{-1} for the AgO$_x$ films of 8 and 12 nm, respectively, whereas the values the FoM of the ITO/Ag/ITO electrode were 2.80×10^{-4} and 1.11×10^{-3} Ω^{-1} for the same thicknesses of the Ag layer. The value of the FoM of the ITO/AgO$_x$/ITO electrode surpassed that of a single 70 nm thick ITO film (2.70×10^{-3} Ω^{-1}) for AgO$_x$ thicknesses equal to or higher than 8 nm. This verified the superior transmittance and conductivity of the ITO/AgO$_x$/ITO electrode using the AgO$_x$ (O/Ag = 2.4 atom %).

The high transmittance of the ITO/AgO$_x$ (O/Ag = 2.4 atom %)/ITO electrode resulted in OSCs fabricated using the electrode and low band gap photoactive polymers exhibiting high conversion efficiencies owing to the expansion of the absorption region of the photoactive polymers to longer wavelengths (up to 750 nm). In the OSCs with an active area (0.36 cm^2), a bulk heterojuction of the photoactive polymers (with polythienothiophene-co-benzodithiophenes 7 F-20 (PTB7-F20) as an electron donor and phenyl-C71-butyric acid methyl ester (PC$_{71}$BM) as an acceptor) was formed on a buffer layer of poly(3,4-ethylenedioxythiophene):poly-(styrenesulfonate) (PEDOT:PSS) resulting in the following configuration: PET/electrode/PEDOT:PSS/PTB7-F20:PC$_{71}$BM/Al (Figure 6a). A comparison of the current density−voltage (J−V) characteristics of the OSCs fabricated using the ITO/AgO$_x$/ITO and ITO/Ag/ITO electrodes showed that the short-circuit current density (J_{sc}) and fill factor (FF) values of the OSCs fabricated using the ITO/AgO$_x$/ITO electrodes were noticeably higher than those of the ITO/Ag/ITO electrode (Figure 6b and Table 1). The higher J_{sc} values of the OSCs fabricated using the ITO/AgO$_x$/ITO electrodes could be mainly attributed to the higher incident-photon-to-current conversion efficiency (IPCE) of the OSCs owing to the optical transmittance of the electrodes being greater for wavelengths between 400 and 750 nm (Figure 6c). The higher work function of the ITO/AgO$_x$/ITO electrodes could cause an additional increase in the J_{sc} value of the OSCs by enhancing the hole-extraction rate from the PEDOT:PSS to the ITO/AgO$_x$/ITO electrodes (Figure 6d). From the secondary cutoff positions of the ultraviolet photoelectron spectroscopy (UPS), the work function of the ITO/AgO$_x$ (8 nm)/ITO electrode was estimated to be 4.63 eV, whereas those of the single ITO film and ITO/Ag (8 nm)/ITO electrodes were 4.32 and 4.39 eV, respectively. The higher work function of the ITO/AgO$_x$/ITO electrode may provide a better energy-level alignment with the HOMO level of PEDOT:PSS and thus facilitate the hole transportation and collection. However, the higher FF values of the OSCs fabricated using the ITO/AgO$_x$/ITO electrodes were due to the fact that their sheet resistance values were lower than those of the ITO/Ag/ITO electrodes. The PCE value for the ITO/Ag (8 nm)/ITO electrode was even lower than that of the single ITO film electrode owing to its poor optical transmittance, although the FF value of the ITO/Ag/ITO electrode was greater than that of the single ITO film electrode. Thus, the high PCE values noticed in the OSCs fabricated using the ITO/AgO$_x$/ITO electrodes were the result of an increase in the photocurrent production owing to the high transmittance of the electrodes for wavelengths in the range 400−750 nm. The PCE value increased by about 25% (i.e., from 4.72 to 5.88%) on replacing the ITO/Ag (8 nm)/ITO electrode with the ITO/AgO$_x$ (8 nm)/ITO electrode.

When the structural durability of the ITO/AgO$_x$/ITO electrode was compared to that of the single ITO film and ITO/Ag/ITO electrodes by exposing them to high compressive stresses induced by the mechanical bending of the PET substrates, the ITO/AgO$_x$/ITO electrode exhibited excellent

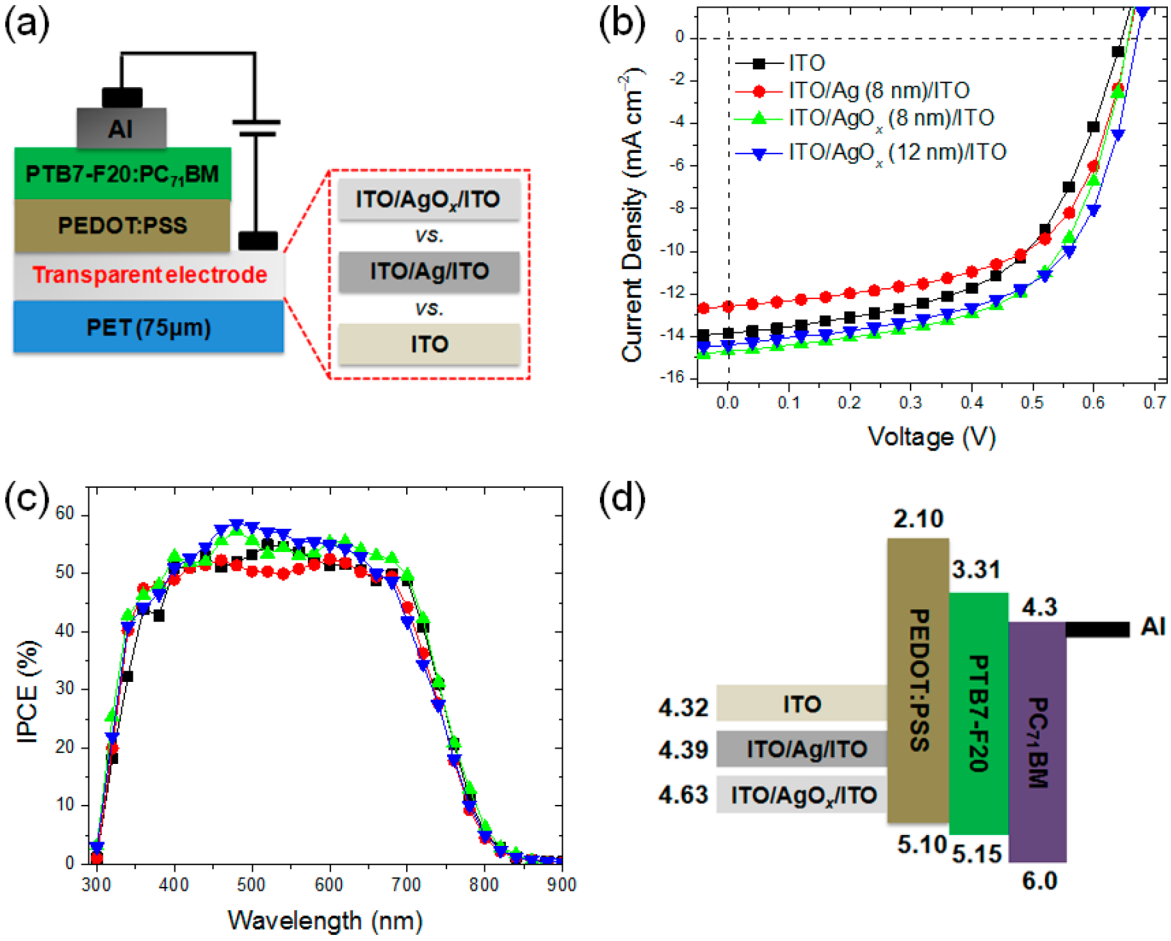

Figure 6. (a) Device architecture of the OSCs used in this study. Comparison of the (b) $J-V$ curves and (c) IPCE spectra of the OSCs fabricated using the different electrodes: ITO/AgO_x (8 and 12 nm)/ITO, ITO/Ag (8 nm)/ITO, and 70 nm thick single ITO film electrodes. (d) Schematic description of the electronic structure of the OSCs.

Table 1. Photovoltaic Performance Parameters of OSCs[a]

electrode	J_{sc} (mA cm^{-2})	V_{oc} (V)	FF (%)	R_{sh} (Ω cm^2)	R_s (Ω cm^2)	PCE (%)
ITO/AgO_x (8 nm)/ITO	14.62 ± 0.31	0.67 ± 0.01	60.33 ± 0.03	2.84 × 10^4	4.21	5.88 ± 0.10
ITO/AgO_x (12 nm)/ITO	14.29 ± 0.35	0.67 ± 0.01	59.88 ± 0.01	2.41 × 10^4	5.13	5.76 ± 0.15
ITO/Ag (8 nm)/ITO	12.53 ± 0.67	0.65 ± 0.01	58.18 ± 0.01	1.56 × 10^4	8.53	4.72 ± 0.17
ITO	13.47 ± 0.47	0.66 ± 0.01	56.75 ± 0.01	2.07 × 10^4	7.31	5.04 ± 0.21

[a]Averaged for five specimens that were determined under simulated AM 1.5G illumination with an irradiance of 100 mW cm^{-2}.

structural durability, which was equivalent to that of the ITO/Ag/ITO electrode. There was no change in the sheet resistance of the ITO/AgO_x/ITO electrode for a bending radius of 2 mm, which corresponded to a compressive strain (ε) of 1.9%, whereas the sheet resistance of the 70 nm thick single ITO film electrode increased by 3.3% for the same bending radius (Figure 7a). The difference in the change in the resistance increased further with further decreases in the bending radius. When the bending radius was decreased to 0.6 mm, the sheet resistance of the ITO/AgO_x/ITO electrode increased by only 13.6%, whereas that of the ITO single film electrode increased by 53.8%. This was due to the development of a number of microscopic cracks in a direction perpendicular to that of the compressive load.[30] The superior mechanical flexibility of the ITO/AgO_x/ITO electrode resulted in the greater mechanical flexibility of the OSCs fabricated using them compared to those fabricated using the single ITO film electrode. The difference in the PCE values of the ITO/AgO_x/ITO and single ITO film electrodes continued to increase with a decrease in the bending radius, with the PCE values decreasing by 17 and 39% in the case of the ITO/AgO_x/ITO and single ITO film electrodes, respectively, for a bending radius of 0.6 nm (Figure 7b).

4. CONCLUSIONS

The inclusion of 2 or 3 atom % oxygen in the Ag layer was enough to cause a sharp increase in the refractive index of the layer without decreasing the electrical conductivity of the OMO electrode comprising an 8−12 nm thick AgO_x film between 30 nm thick films of ITO. The increase in the refractive index of AgO_x directly resulted in the improvement of the optical transmittance of the OMO electrode owing to better optical matching between the AgO_x and ITO films. As a result of the improvement in the transmittance because the oxidization of Ag was more significant with respect to longer wavelengths in the visible spectral range, the difference in the transmittance of

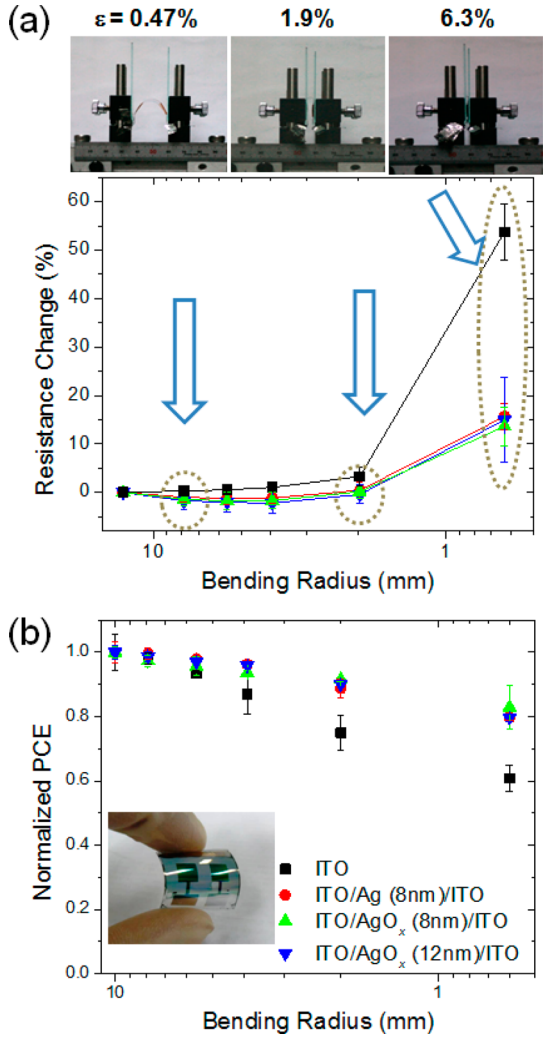

Figure 7. (a) Percentage change in the resistance of the electrodes and (b) normalized PCE values of the fabricated OSCs using the electrodes as a function of the bending radius during the irreversible bending tests.

the ITO/AgO$_x$ (O/Ag = 2.4 tom %)/ITO and ITO/Ag/ITO electrodes increased with an increase in the wavelengths tested and reached a value of 30% for wavelengths greater than 600 nm. The high transmittance of the ITO/AgO$_x$/ITO electrode resulted in improvements in the power-conversion efficiencies of OSCs fabricated using the electrode owing to an increase in the current density. For OSCs having the configuration PET/electrode/PEDOT:PSS/PTB7-F20:PC$_{71}$BM/Al, the use of the ITO/AgO$_x$ (8 nm)/ITO electrode resulted in a power-conversion efficiency of 5.88%. This was almost 25% higher than that for the OSCs fabricated using the ITO/Ag (8 nm)/ITO electrode. To our knowledge, a power-conversion efficiency of 5.88% is the highest ever reported for OSCs fabricated on highly flexible and heat-sensitive polymer substrates.[31] Furthermore, OSCs fabricated using the ITO/AgO$_x$ (8 nm)/ITO electrode continued to exhibit a power-conversion efficiency of 5% even when subjected to an extremely high compressive strain of about 6.3%, which was induced by the mechanical bending of the PET substrate with a bending radius of 0.6 mm.

■ ASSOCIATED CONTENT

Ⓢ Supporting Information

Total (and specular) transmittance and reflection of single Ag and AgO$_x$ films. Top-view FE-SEM images of Ag and AgO$_x$ films on ITO films, ITO/Ag/ITO, and ITO/AgO$_x$/ITO electrodes. Sheet resistances of single ITO film electrodes deposited on polymer substrates with different film thicknesses. Figure of merit of ITO/Ag/ITO and ITO/AgO$_x$/ITO electrodes. This material is available free of charge via the Internet at http://pubs.acs.org.

■ AUTHOR INFORMATION

Corresponding Authors

*E-mail: jungheum@kims.re.kr (J.Y.). Tel: +82 (0)552803515. Fax: +82 (0)552803570.
*E-mail: smk1017@kims.re.kr (M.S.). Tel: +82 (0)552803676 . Fax: +82 (0)552803570.
*E-mail: jwkang@jbnu.ac.kr (J.-W.K.).

Notes

The authors declare no competing financial interest.

■ ACKNOWLEDGMENTS

This research was funded by the World Premier Materials (WPM) program and by internal grants from the Korea Institute of Materials Research. W.W. thanks the China Scholarship Council for financial support. The authors thank Prof. M. S. Kwon of the Ulsan National Institute of Science and Technology for a valuable discussion on the optical properties. The authors also thank Y. Hwang of the Electronics and Telecommunications Research Institute (ETRI) for her help with the XPS measurements. The ellipsometric measurements to determine the refractive indices were carried out at Ellipso Technology Co. Ltd.

■ REFERENCES

(1) Lewis, J.; Grego, S.; Chalamala, B.; Vick, E.; Temple, D. *Appl. Phys. Lett.* **2004**, *85*, 3450−3452.
(2) Han, H.; Theodore, N. D.; Alford, T. L. *J. Appl. Phys.* **2008**, *103*, 013708-1−013708-8.
(3) Indluru, A.; Alford, T. L. *J. Appl. Phys.* **2009**, *105*, 123528-1−123528-9.
(4) Sivaramakrishnan, K.; Alford, T. L. *Appl. Phys. Lett.* **2009**, *94*, 052104-1−052104-3.
(5) Park, Y. S.; Choi, K. H.; Kim, H. K. *J. Phys. D: Appl. Phys.* **2009**, *42*, 235109.
(6) Guillén, C.; Herrero, J. *Phys. Status Solidi A* **2010**, *207*, 1563−1567.
(7) Chakaroun, M.; El Amrani, A.; Lucas, B.; Ratier, B.; Aldissi, M. *Eur. Phys. J.: Appl. Phys.* **2010**, *51*, 33206-1−33206-5.
(8) Kuang, P.; Park, J.-M.; Leung, W.; Mahadevapuram, R. C.; Nalwa, K. S.; Kim, T.-G.; Chaudhary, S.; Ho, K.-M.; Constant, K. *Adv. Mater.* **2011**, *23*, 2469−2473.
(9) Lee, J.-Y.; Connor, S. T.; Cui, Y.; Peumans, P. *Nano Lett.* **2008**, *8*, 689−692.
(10) Azulai, D.; Belenkova, T.; Gilon, H.; Barkay, Z.; Markovich, G. *Nano Lett.* **2009**, *9*, 4246−4249.
(11) Hu, L.; Kim, H. S.; Lee, J.-Y.; Peumans, P.; Cui, Y. *ACS Nano* **2010**, *4*, 2955−2963.
(12) Wu, Z. C.; Chen, Z. H.; Du, X.; Logan, J. M.; Sippel, J.; Nikolou, M.; Kamaras, K.; Reynolds, J. R.; Tanner, D. B.; Hebard, A. F.; Rinzler, A. G. *Science* **2004**, *305*, 1273−1276.
(13) Hu, L.; Hecht, D. S.; Grüner, G. *Nano Lett.* **2004**, *4*, 2513−2517.
(14) Dan, B.; Irvin, G. C.; Pasquali, M. *ACS Nano* **2009**, *3*, 835−843.

(15) Becerril, H. A.; Mao, J.; Liu, Z.; Stoltenberg, R. M.; Bao, Z.; Chen, Y. *ACS Nano* **2008**, *2*, 463−470.
(16) Eda, G.; Lin, Y. Y.; Miller, S.; Chen, C. W.; Su, W. F.; Chhowalla, M. *Appl. Phys. Lett.* **2008**, *92*, 233305-1−233305-3.
(17) Wang, X.; Zhi, L.; Müllen, K. *Nano Lett.* **2008**, *8*, 323−327.
(18) Wan, Q.; Dattoli, E. N.; Fung, W. Y.; Guo, W.; Chen, Y.; Pan, X.; Lu, W. *Nano Lett.* **2006**, *6*, 2909−2915.
(19) O'Dwyer, C.; Szachowicz, M.; Visimberga, G.; Lavayen, V.; Newcomb, S. B.; Sotomayor Torres, C. M. *Nat. Nanotechnol.* **2009**, *4*, 239−244.
(20) Yu, H. K.; Dong, W. J.; Jung, G. H.; Lee, J.-L. *ACS Nano* **2011**, *5*, 8026−8032.
(21) Tominaga, J. *J. Phys.: Condens. Matter* **2003**, *15*, R1101−R1122.
(22) Barik, U. K.; Srinivasan, S.; Nagendra, C. L.; Subrahmanyam, A. *Thin Solid Films* **2003**, *429*, 129−134.
(23) Abe, Y.; Hasegawa, T.; Kawamura, M.; Sasaki, K. *Vacuum* **2004**, *76*, 1−6.
(24) Pierson, J. F.; Wiederkehr, D.; Billard, A. *Thin Solid Films* **2005**, *478*, 196−205.
(25) Rivers, S. B.; Bernhardt, G.; Wright, M. W.; Frankel, D. J.; Steeves, M. M.; Lad, R. J. *Thin Solid Films* **2007**, *515*, 8684−8688.
(26) Al-Kuhaili, M. F. *J. Phys. D: Appl. Phys.* **2007**, *40*, 2847−2853.
(27) Park, S. I.; Ahn, J. H.; Feng, X.; Wang, S.; Huang, Y.; Rogers, J. A. *Adv. Funct. Mater.* **2008**, *18*, 2673−2684.
(28) Novotny, L., Hecht, B. *Principles of Nano-Optics*, 1st ed.; Cambridge University Press: Cambridge, 2006; Chapter 10.
(29) Haacke, G. *J. Appl. Phys.* **1976**, *47*, 4086−4089.
(30) Leterrier, Y.; Médico, L.; Demarco, F.; Månson, J.-A. E.; Betz, U.; Escolà, M. F.; Kharrazi Olsson, M.; Atamny, F. *Thin Solid Films* **2004**, *460*, 156−166.
(31) Guillén, C.; Herrero, J. *Thin Solid Films* **2011**, *520*, 1−17.